JREE: Vol. 9, No. 4, (Autumn 2022) 64-75

Journal of Renewable Energy and Environment

Journal Homepage: www.jree.ir

Materials and Energy Research Center

MERC

Research Article

Numerical Modeling and Evaluation of a Downwind Pre-Aligned Wind Turbine with an Innovative Blade Geometry Concept

Amir Hossein Zare [a,b], Esmail Mahmoodi [c*], Mohsen Boojari [a], Ali Sarreshtehdari [a]

[a] Department of Mechanical Engineering, Shahrood University of Technology, P. O. Box: 3619995161-316, Shahrood, Semnan, Iran.
[b] Fars Power Generation Management Company, Shiraz, Fars, Iran.
[c] Department of Mechanical Engineering of Biosystem, Shahrood University of Technology, P. O. Box: 3619995161-316, Shahrood, Semnan, Iran.

PAPER INFO

Paper history:
Received: 03 October 2021
Revised in revised form: 27 January 2022
Scientific Accepted: 27 February 2022
Published: 04 September 2022

Keywords:
Extreme-Scale Wind Turbines,
Pre-Aligned Rotor,
CFD Simulation,
Wake Simulation

ABSTRACT

Significant growth of the wind power market has led to a dramatic increase in the scale and capacity of wind turbines over the past decades. As these extreme-scale structures are expected to pose a wide range of challenges, an innovative concept which both lightens blade's mass and improves their aerodynamic performance, is vital for the future of rotor's design. In the present study, modeling and evaluating of an innovative pre-aligned rotor design based on SANDIA SNL100-00 wind turbine blade were accomplished. To evaluate the aerodynamic performance of the proposed rotor, CFD simulation was used as a well-developed technique in fluid mechanic. In the new rotor design, the swept area was increased using an equal blade length and the blade sections were more appropriately aligned with the wind flow compared to the reference model. This enhancement attained due to transferring the bending position from the root to a certain point alongside the length of blade. According to simulation assessments, this modification led to the overall improvement of main performance parameters in terms of the mean power and the applied torque on the blades. The simulation revealed that the novel concept is capable of increasing the mean power coefficient by 13.21 % compared to the conventional rotor designs. Analysis of the axial induction in front of the rotor plane displayed a greater drop in the flow velocity streaming up to the rotor, which could lead to have a more efficient configuration for harnessing the upcoming wind's power.

https://doi.org/10.30501/jree.2022.306692.1264

1. INTRODUCTION

Renewable energy systems have witnessed an increase in power generation capacity over the last years. Given that this growth is envisioned to continue, it is expected of future systems to have rated power in the range of 10-20 megawatt and a rotor diameter of 170 to 240 meters in order to decrease the Levelized Cost of Energy (LCOE) [1]. This means that modern wind turbines designed for offshore application would become the most gigantic rotary system on earth, with the length of one blade at least equal to the entire wing of a Boeing 747 [2]. To achieve these dimensions, several design factors in different fields including aerodynamics, structures, and active or passive control systems need to be simultaneously considered in the design process of large-scale turbines [3].

Various scientific research works including Fischer [4] have focused on this research area and explored different airfoil designs to reduce the overall loads on the blade. Studies by Sartori [5] and Griffith [6] have shown promising results through optimizing blades to provide a good starting point to design wind turbine blades. Deshmukh et al. [7] introduced an integrated approach to optimizing the wind turbine design by applying a co-design method; a design procedure that accounts directly for the synergistic coupling between physical and control system design. It was shown that employing a multidisciplinary strategy would result in the performance improvement of up to 8 % compared to conventional sequential design methods.

Wind turbines harness wind energy with the purpose of power generation which is scaled with V_{wind}^3 However, the fabrication, transportation, and assembly processes of extreme-scale turbines face wide-ranging obstacles. In particular, the most critical issue for conventional rotor configurations on large scales is the blade's mass. It is worth mentioning that the blade mass increases cubically or sub-cubically with its length [8]. For example, it is estimated that the mass per blade could exceed 75,000 kg for a 20 megawatt three-bladed turbine [9]. Hence, blade mass saving is essential to the designing and manufacturing of these wind turbines.

Various approaches have been applied with the aim of blade lightening. These methods could be classified into two groups.

*Corresponding Author's Email: esmail.mahmoodi@gmail.com (E. Mahmoodi)
URL: https://www.jree.ir/article_156017.html

Please cite this article as: Zare, A.H., Mahmoodi, E., Boojari, M. and Sarreshtehdari, A., "Numerical modeling and evaluation of a downwind pre-aligned wind turbine with an innovative blade geometry concept", ***Journal of Renewable Energy and Environment (JREE)***, Vol. 9, No. 4, (2022), 64-75. (https://doi.org/10.30501/jree.2022.306692.1264).

The first type of solution involves using advanced material and structure design. Carbon fiber material is utilized to replace a portion of the glass fiber-reinforced plastics due to the carbon fiber's high strength and low density [10, 11]. Nonetheless, the expensive cost of stronger materials has curbed their applicability.

The other practical methods are those that reduce the material demands by alleviating the aerodynamic loads exerted on turbine blades. This set of methods involves optimization of the blade plies, location, and thickness [12, 13], flexible pre-aligned rotor [14, 15], adaptable blade geometry [9, 16], and the morphing blade with the flap or smart structure [17-22].

In this regard, two novel concepts have been developed based on load-alignment for extreme-scale systems namely Segmented Ultralight Morphing Rotors (SUMR) [23] and Segmented Ultralight Pre-aligned Rotors (SUPAR) [24]. Both models introduce a load alignment strategy that orients the loads along the blade span-wise direction to significantly reduce the bending moments at the root. Upon taking full advantage of the load reduction in the SUMR concept, a number of challenges in developing extreme-scale wind turbines can potentially be addressed [25]. There are prominent research works that have been dedicated to investigating conceptual design, aerodynamics, and control system design of the SUMR wind turbines [26-28].

As an example, Noyes et al. [29] proposed a two-bladed downwind morphing rotor that was compared with a three-bladed conventional upwind rotor. The simulation results indicated that their SUMR rotor could bring about 27 % material saving and 8.56 % reduction in the blade lifetime damage in return for a 0.5 % decrease in the average generated power. Similarly, Ichter et al. [30] introduced a Morphing Downwind-Aligned Rotor (MDAR) in which the rotor had stiff elements in blades. Besides, to provide moment-free alignment in downwind conditions, they considered hub-joints in the rotor configuration. They observed that the morphing idea would increase the energy capture in low-speed conditions even though coning and reduction of blade number result in the reduction of rated power. Additionally, it was reported that the alignment of the centrifugal, gravitational, and thrust forces with the direction of the blade's path would reduce the cantilever loads.

In addition to the above research works, a deeper insight is provided herein by reviewing several studies to investigate the idea of load-alignment for rotors on extreme scales.

Loth et al. [9, 24] proposed a downwind rotor design with regard to the load-alignment concept. In their plan, since blades generally tolerate the exerted tensional force, they experience fewer bending moments than conventional types. Moreover, application of load-alignment to downwind turbines with larger tower clearance removed the rotor-tower clearance constraint, which allowed more flexible and lighter blades to be manufactured. Employing this concept for a two-bladed rotor resulted in a mass reduction of about 27 % based on a 13.2 MW reference rotor [26, 31]. Qin et al. [32] upscaled the load-aligned design from 13.2 MW to 25 MW with a downwind two-bladed configuration. Additionally, they employed a fully redesigned 25 MW model to demonstrate the capability of integrating morphing to harness even more wind energy while limiting the applied loads. In parallel, segmented blades and outboard pitching ideas were examined as a promising solution to overcome the increased edge-wise loads of load-alignment. Similarly, Yao et al. [33] attempted performing an aero-structural design study to achieve a 50 MW two-bladed wind turbine with a rotor diameter exceeding than 500 m. Their research involved initial study and investigations of structural design and performance of a baseline 250 m blade, along with implementing an optimization strategy to satisfy the need for a mass/cost-reduced rotor design. The optimization process, accomplished by investigating different airfoil thickness designs and chord designs, resulted in more than a 25 % mass reduction and saved over 30 % in overall cost.

Bortolotti et al. [34] compared 10 MW upwind and downwind three-bladed rotors, with and without active cone control. It was reported that although downwind rotors benefited from reduced cantilever loadings, no evident advantages were seen compared to upwind designs. To sum up, discussion of the downwind and load-alignment concepts continues and the switch to downwind designs demands further research.

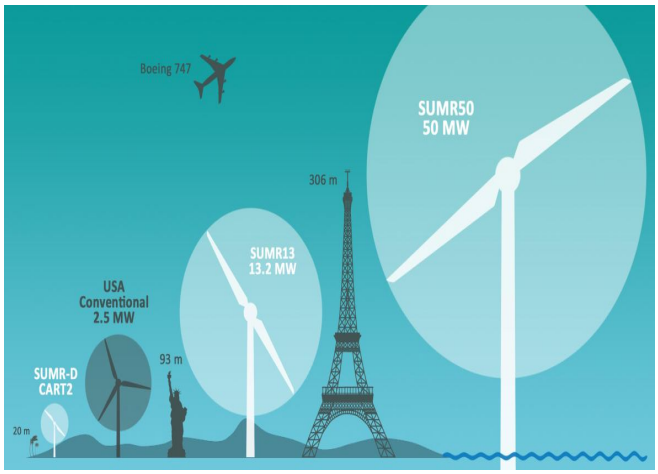

Figure 1. Schematic view of a 50 MW wind turbine and comparison of its size with a 13.2 MW two-bladed downwind turbine and conventional 2.5 MW three-bladed upwind turbine [33]

Taking advantage of previous studies concerning new concepts for large-scale rotors, a new downwind, pre-aligned rotor with a novel blade configuration referred to as "bent blade" has been proposed in this paper. Unlike prior pre-aligned rotor concepts, the proposed blades are not deformed or bent from a particular point in the span-wise direction; instead, they are slightly angled from the root toward the hub by inserting a special joint at the hub. The novelty of the current study lies in determining the location of the blade's bending point. In this research, the blade's bending point is designated somewhere between the cylindrical section and the very first airfoil profile. Moreover, a series of parameters in terms of power coefficient, thrust force, and applied torque on the blades are calculated and compared to conventional blade design in an attempt to evaluate the aerodynamic performance of the proposed concept.

The topics addressed in this paper include definition of load-alignment concepts in extreme-scale wind turbines in Section 2, highlighting the importance of this issue in the design process. Section 3 presents the simulation methodology that describes the fundamental equations, turbulence modeling, CAD design procedure, meshing strategy, and boundary conditions. Section 4 provides the corresponding CFD (computational fluid dynamics) results for the proposed rotor concept in terms of aerodynamic performance parameters. Section 5 presents the results and discussion.

2. LOAD ALIGNMENT AND FORCE DISTRIBUTION

The load alignment concept is inspired by nature, especially the flow adaptability of certain trees. For instance, the natural aero-elastic design of palm trees reduces aerodynamic loads while maintaining structural mass at its minimum. Under moderate wind conditions, the flexible configuration can bend downstream and alleviate destructive cantilever aerodynamic loads [35]. Similarly, since cantilever loads are extremely significant for large-scale wind turbines, the alignment allows a greater reduction of moments experienced by rotor blades.

There are two main methods to apply the load alignment concept: (a) to set a constant pre-cone angle to obtain load alignment in one specific condition (pre-aligned) and partial alignment in other conditions using aeroelastic deflection; (b) to make use of a hinge configuration that provides active full-load alignment by changing the coning angle as a function of wind speed. Since the pre-aligned technique reduces the need for an additional actuator, hinge, and controller, it is more straightforward for implementation. On the other hand, the active coning method can moderate the flap-wise bending moment for a wider range of wind speeds.

As mentioned before, this concept is capable of reducing rotor mass through disregard for the conventional stiffness constraint and alternatively, adjusting a downwind geometry to ensure alignment with the load path [9], as shown in Figure 2. Here, it is seen that the conventional blade loading leads to cantilever forces in the downstream direction. In contrast, the aligned concept employs a geometry that orients the loads in the span-wise direction so that the structural loads can be mainly exerted in the tension mode. The resulting load-path angles (β) slightly vary as a function of radius and azimuthal angle. By converting loads to tensile, this concept effectively reduces mass by minimizing cantilever-based shear loads [9].

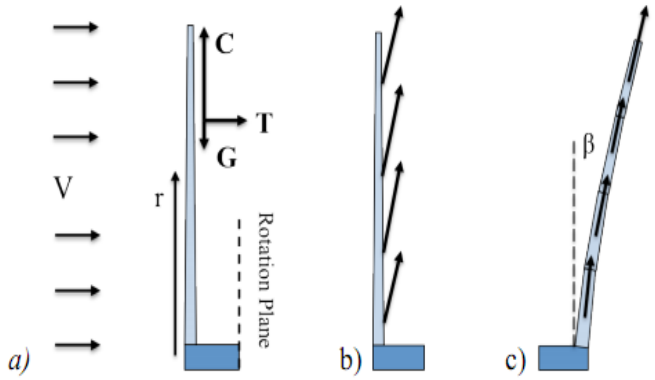

Figure 2. a) The non-torque forces on the blade of a wind turbine; b) net-force distribution in a conventional upwind blade; c) force distribution of a SUMR blade [32]

The spanwise load-path angle (β) can be quantified as a function of blade azimuthal angle (φ) using Equation (1) [1]:

$$\beta = \tan^{-1}\left(\frac{T}{C - G\cos\varphi}\right) \quad (1)$$

where T is the downstream aerodynamic thrust force, C the centrifugal force, and G the gravity force. The blade azimuthal angle (φ) is defined as 0 for a blade that is pointed vertically upwards and π for a blade that is pointed downwards. Of note, the load-path angles (β) for extreme-scale turbines are large, e.g., can be more than 20° for a 20 MW system [1]. As a system approaches extreme scales, not only downwind cantilever stresses but also gravity stresses get larger and more challenging for the conventional rotor design. However, both of these problems can be mitigated with the downstream curvature aligned with these forces, as shown in Figure 2(c).

In terms of aerodynamic force, the load alignment concept involves finding a balance between the downwind thrust force and the radial centrifugal force in an attempt to align the longitudinal axis with the net resultant force [36, 37]. The decomposition of forces acting on a turbine blade along with its resultant force for a downwind Coned rotor is shown in Figure 3. These forces include the gravity force (FG), the centrifugal force (FC), the downstream aerodynamic thrust force (FT), where all summed into resultant force (FR), and the in-plane aerodynamic torque-wise force (FQ). Note that the latter two forces result from the lift force (L) if drag (D) is neglected.

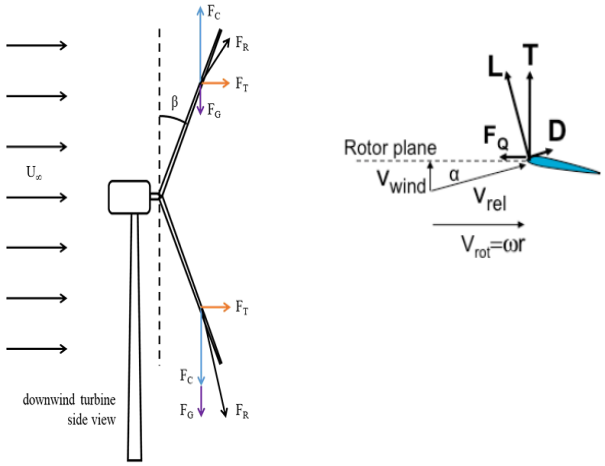

Figure 3. Forces and velocities for a horizontal wind turbine blade from a) side-view [29], b) chord-wise

The integrated transverse force, which is a function of coning angle, leads to root flap-wise bending moments. Load alignment decreases the flap-wise bending moments by setting the coning angle such that the contributions from the centrifugal and thrust loads are roughly eliminated. This can merely be achieved when coning is in the direction of the wind as in the case of a downwind rotor so that the centrifugal component is upwind and opposite to the downwind thrust component. While load alignment does not directly lower the lead-lag bending moments, the rotor mass reduction may cause lower gravity load and accordingly, lower lead-lag bending load [29].

3. SIMULATION METHODOLOGY

3.1. Governing equations

3.1.1. Incompressible Navier-Stokes equations

In the last decade, Wind Turbine Computational Fluid Dynamics (WTCFD) are substantially concentrated on solving Navier-Stokes equations in incompressible conditions. The freestream velocity passing wind turbines varies between 5 and 25 m/s, which is categorized as incompressible. Traces of compressibility could be seen at the blades' tips due to high-speed rotations. Mach number at the tip is lower than 0.25, which explains the possibility of neglecting compressibility.

Therefore, Navier-Stokes equations in incompressible conditions, as in Equations (2) and (3), are suitable for wind turbine modeling [38].

$$\nabla . u = 0 \tag{2}$$

$$\frac{\partial u}{\partial t} + (u.\nabla)u = -\frac{1}{\rho}\nabla p + \nu\nabla^2 u \tag{3}$$

where u is the velocity, ρ the density, p the pressure, t the time, and ν the kinematic viscosity.

3.1.2. Aerodynamic performance of wind turbines

3.1.2.1. Thrust coefficient

Thrust is the axial force that is applied by the wind to a rotor disk. While the power output of a wind turbine describes only the amount of power transferred into the electrical system, the thrust is related to all the losses of the kinetic energy of the flow, including the energy transformed into turbulent kinetic energy [39]. It must be considered that a lower thrust is beneficial, since less construction material would be needed to strengthen the supporting tower. Coefficient of thrust (C_T) is a non-dimensionalized parameter that represents the force on an actuator disc (turbine's rotor) caused by the pressure drop and it can be expressed using Equation (4) [40]:

$$C_T = \frac{T}{\frac{1}{2}\rho U_\infty^2 A_d} \tag{4}$$

where ρ is the air density, A_d the rotor cross-sectional area, and U_∞ the far upstream flow velocity.

3.1.2.2. Generated torque

Torque is a crucial parameter that affects different aspects of the performance of a wind turbine including the ability to overcome the resistive torque induced by friction [41]. According to Burton et al. [39], the total driving torque (Q) which a wind turbine rotor is capable of developing can be defined through Equation (5):

$$Q = \frac{1}{2}\rho U_\infty^2 \pi R^3 \lambda \left[\int_0^R \mu^2 \left[8á(1-a)\acute{\mu} - \frac{W}{U_\infty}\frac{B\frac{c}{R}}{\pi} C_d(1+á)\right] d_\mu\right] \tag{5}$$

Herein, λ represents tip speed ratio, a and á are axial and tangential flow induction factors, respectively, W relative wind velocity, B the number of blades, c the chord length, C_d the drag coefficient, and the parameter $\mu = {}^{r}/_{R}$.

3.1.2.3. Turbine power

The available power of the wind with speed U_∞ through a cross-sectional area A is defined as follows:

$$P = \frac{1}{2}\rho U_\infty^3 A \tag{6}$$

The shaft extracted power of a wind turbine can be represented by the following equation:

$$P = \frac{1}{2} C_p \rho U_\infty^3 A \tag{7}$$

where C_p is a dimensionless variable called power coefficient, which is calculated to deduce the aerodynamic efficiency of a wind turbine. According to Betz theory [42], the maximum theoretical value of C_p is 0.593, which is called Betz limit. Power coefficient depends on several parameters including the free stream velocity, the electrical and mechanical efficiencies of the generator, the drag force magnitude, and the viscosity on the blade's surface. In this study, the overall electrical and mechanical efficiencies of the generator and shaft are assumed to be 0.9, as stated by Loth et al. [9]. Considering the above equations, the coefficient of power can fairly be defined as [39]:

$$C_p = \frac{\text{Power Extracted}}{\text{Power Available}} = \frac{Q\Omega}{\frac{1}{2}\rho U_\infty^3 \pi R^2} \tag{8}$$

where Q denotes total driving torque on the rotor shaft, Ω rotational speed of rotor, and R blade radius.

3.1.3. Turbulence modeling

Over the years, various two-equation turbulence models have been introduced to study the flow field around wind turbines. In the present work, Menter's k-ω Shear-Stress Transport (SST) model [43] is employed. This turbulence model uses k-ω model [44] in the inner region of the boundary layer and switches to k-ε model [45] in the free shear flow to enhance the prediction of adverse pressure gradients. The change is smoothly controlled by the weight function of the coefficients on both models. The primary equations are written as follows [42]:

$$\frac{D\rho k}{Dt} = \tau_{ij}\frac{\partial u_i}{\partial x_j} - \beta^*\rho\omega k + \frac{\partial}{\partial x_j}\left[(\mu + \sigma_k\mu_t)\frac{\partial k}{\partial x_j}\right] \tag{9}$$

$$\frac{D\rho\omega}{Dt} = \frac{\gamma}{\nu_t}\tau_{ij}\frac{\partial u_i}{\partial x_j} - \dot{\beta}\rho\omega^2 + \frac{\partial}{\partial x_j}\left[(\mu + \sigma_\omega\mu_t)\frac{\partial \omega}{\partial x_j}\right] + 2\rho(1 - F_1)\sigma_{\omega 2}\frac{1}{\omega}\frac{\partial k}{\partial x_j}\frac{\partial \omega}{\partial x_j} \tag{10}$$

where k is turbulence kinetic energy, ω turbulent frequency, τ_{ij} turbulent Reynolds stress tensor, μ_t eddy viscosity, ν_t kinematic eddy viscosity, (γ, σ, β^*, $\dot{\beta}$) represent turbulence modeling constants, and F_1 denotes the blending function which is designed to be a value of one in the near-wall region and zero far from the wall.

3.2. Model setup

3.2.1. CAD design of a pre-aligned blade

Griffiths et al. [46] developed a methodology to design a blade with a 100-meter length, used in the SANDIA SNL100-00 wind turbine, to serve as a baseline for future researches. This blade was employed to model and simulate a pre-aligned rotor in a study by Loth et al. [1], which is the validation reference of the current study. The structural properties of SANDIA are given in Table 1.

3.2.2. CAD modeling of the coned blade (verification blade)

Re-simulation of one of the previous studies as the reference frame was required to validate the results of the current research. To this end, the 112.7 m length blade of a Downwind Pre-Aligned wind turbine (D2PAL) introduced by Loth et al. [1] was modeled in CATIA. The dimensions, as well as the coning angle of this blade, are presented in Figure 4.

Table 1. Blade geometry and properties of SANDIA SNL100-00

Section	Blade fraction	Chord (m)	Twist (deg)	Pitch axis (fraction)	Distance from pitch axis (m)	Transition	Airfoil description
1	0	5.694	13.308	0.5	0	0	Cylinder
2	0.005	5.694	13.308	0.5	0	0	Cylinder
3	0.007	5.694	13.308	0.5	0	99.25	Trans 99.25 %
4	0.009	5.694	13.308	0.5	0	98.5	Trans 98.5 %
5	0.011	5.694	13.308	0.5	0	97.75	Trans 97.75 %
6	0.013	5.64	13.308	0.5	0	97	Ellipse 97 %
7	0.024	5.792	13.308	0.499	0.0058	93.1	Ellipse 93.1 %
8	0.026	5.811	13.308	0.498	0.0116	92.5	Ellipse 92.5 %
9	0.047	6.058	13.308	0.483	0.103	84	Trans 84 %
10	0.068	6.304	13.308	0.468	0.2017	76	Trans 76 %
11	0.089	6.551	13.308	0.453	0.3079	68	Trans 68 %
12	0.114	6.835	13.308	0.435	0.4443	60	Trans 60 %
13	0.146	7.215	13.308	0.41	0.6494	51	Trans 51 %
14	0.163	7.407	13.177	0.4	0.7407	47	Trans 47 %
15	0.179	7.552	13.046	0.39	0.8307	43.5	Trans 43.5 %
16	0.195	7.628	12.915	0.38	0.9154	0	Du99-w-405
17	0.222	7.585	12.133	0.378	0.9254	38	Du99-w-405 (38 %)
18	0.249	7.488	11.35	0.377	0.921	36	Du99-w-350 (36 %)
19	0.276	7.347	10.568	0.375	0.9184	34	Du99-w-350 (34 %)
20	0.358	6.923	9.166	0.375	0.8654	0	Du97-w-300
21	0.439	6.942	7.688	0.375	0.8678	26	Du91-w2-250 (26 %)
22	0.52	5.915	6.18	0.375	0.7394	23	Du93-w-210 (23 %)
23	0.602	5.417	4.743	0.375	0.6771	0	Du93-w-210
24	0.667	5.019	3.633	0.375	0.6274	19	Naca-64-618 (19 %)
25	0.683	4.92	3.383	0.375	0.615	18.5	Naca-64-618 (18.5 %)
26	0.732	4.621	2.735	0.375	0.5776	0	Naca-64-618
27	0.764	4.422	2.348	0.375	0.5528	0	Naca-64-618
28	0.846	3.925	1.38	0.375	0.4906	0	Naca -64-618
29	0.894	3.619	0.799	0.375	0.4524	0	Naca -64-618
30	0.943	2.824	0.28	0.375	0.353	0	Naca -64-618
31	0.957	2.375	0.21	0.375	0.2969	0	Naca -64-618
32	0.972	1.836	0.14	0.375	0.2295	0	Naca -64-618
33	0.986	1.208	0.07	0.375	0.151	0	Naca -64-618
34	1	0.1	0	0.375	0.0125	0	Naca -64-618

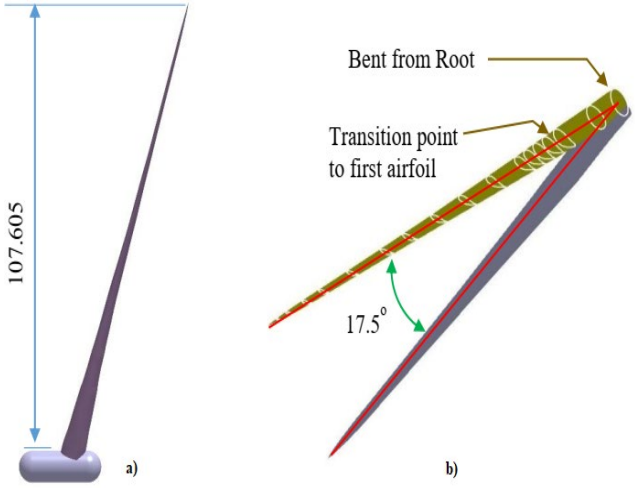

Figure 4. Geometry and dimensions of D2PAL blade: a) side view and b) isometric view

3.2.3. Modeling the bent blade in CATIA

The proposed blade in the present study is of the same length and airfoil sections as the verification blade, but the distinctive difference is contemplated in the bending location. While the D2PAL blade is angled from the hub root, the bent blade has a 17.5° bend in the transition area between the cylindrical section and the elliptic airfoil. The final designed model is shown in Figure 5.

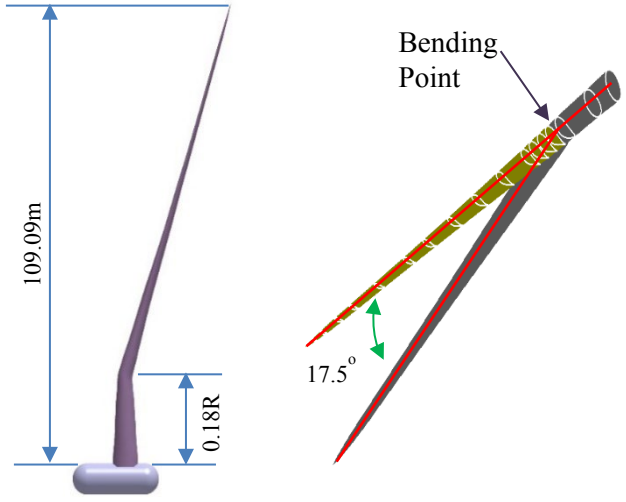

Figure 5. Geometry and dimensions of the proposed blade designed in CATIA

3.2.4 Computational setup

The computational domain and subsequently, the associate mesh are divided into two sections thanks to the solution domain's symmetric geometry. Thus, the flow analysis was performed only in one of the halves. The most prominent step in pre-processing is the generation of grids. It is crucial to employ accurate grids in the solver to acquire precise results.

In the present simulation, an unstructured triangular mesh of average orthogonal quality of 0.90 and a total number of 20 million cells and 4,340,843 nodes was applied to the geometry. To ensure that the blade surface is pinpointed within the viscous sublayer, the very first elements should be close enough to the wall so as to yield y pluses ideally close to 1. Therefore, 20 inflation layers with a growth rate of 1.2 were applied to the blade surface. It must be noted that the first elements next to the blade surface have a thickness of only 2.7 × 10−5 meters. Figure 6 illustrates the applied mesh on the two more challenging regions of the blade geometry.

y+ indicates the dimensionless distance from the wall measured in terms of viscous length on the boundary layer. y+ can be calculated using Equation (11) in which y is the distance from the wall, u_t the friction velocity, and ν the kinematic viscosity.

$$y^+ = \frac{yu_t}{\nu} \quad (11)$$

According to Figure 7, y+ values lie within 0 to 5 in the generated mesh in all three directions. This is enough to fulfill the near-wall requirement, which states that y+ should be kept under 5 for the SST k-ω model [47].

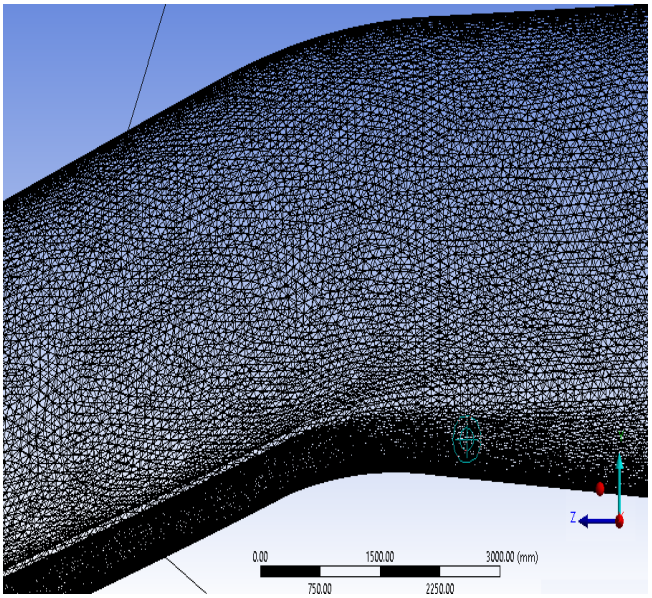

(a)

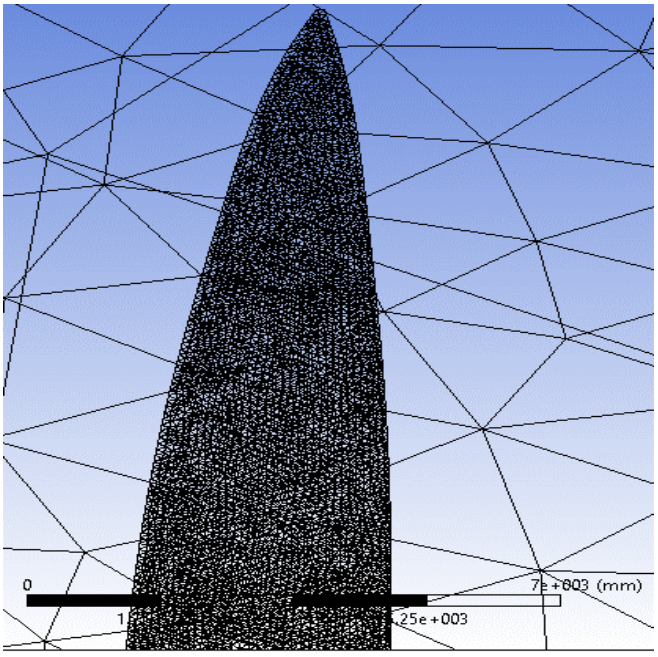

(b)

Figure 6. Applied unstructured triangular mesh on the blade geometry at a) bending point and b) blade tip

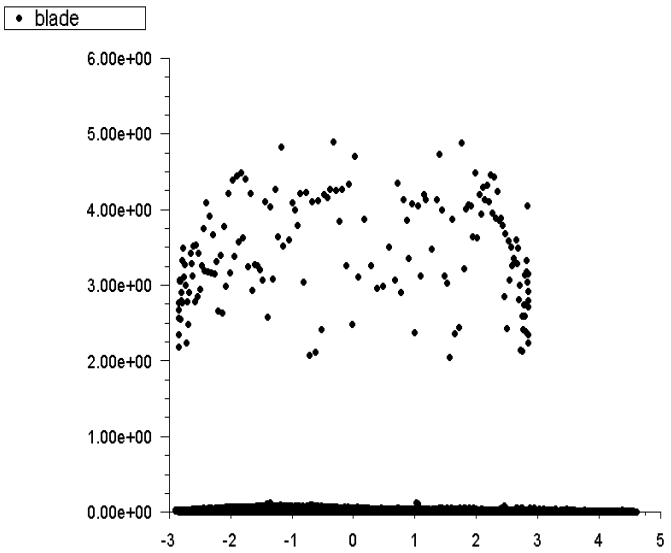

Figure 7. y^+ values of the designed blade in the chord-wise direction

Once the 3D model of the turbine's rotor and the solution domain are created, their corresponding Boundary Conditions (BC) must be defined. The boundary conditions must be accurately specified to secure a reliable simulation. The solution domain and applied boundary conditions are illustrated in Figure 8.

According to Figure 8, the velocity-inlet condition is assigned to face A. With reference to the study of Loth et al. [1], the input velocity for the turbine in the rated conditions is decided to be 14.125 m/s. Further simulations are also conducted at different freestream velocities ranging between 7-24 m/s, equivalent to the tip speed ratio (λ) of 4-15 in which λ is defined through Equation (12). The pressure outlet condition was selected for face C.

A: Velocity inlet
B: Symmetry
C: Pressure outlet
D: Periodic
E: Periodic
F: Body-sizing
G: Blade

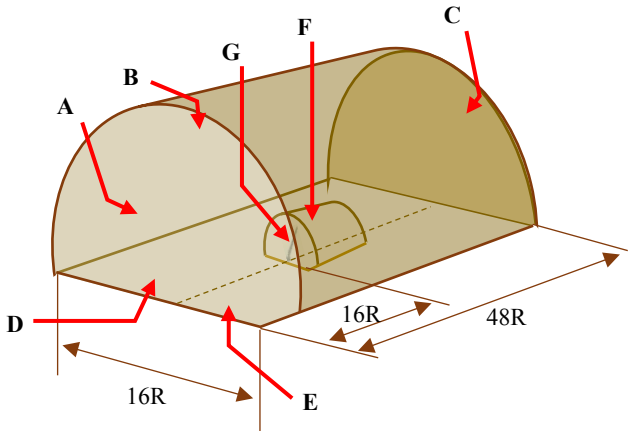

Figure 8. Dimensions and Boundary conditions of the computational domain (R is blade radius)

This is because this boundary condition is applied only to the flow exits, where the flow velocity and/or the pressure details are unknown. The no-slip or the wall condition set for face G is employed to capture solid and fluid regions, which are the surfaces of the blade and the surrounding air. The symmetry boundary condition was selected for face B because its corresponding physical geometry was somehow mirrored in symmetry. As in the current study, the tower effect is neglected and the geometry of each blade is identical. The physical geometry and the flow pattern seem to have a periodically repeating cycle. Therefore, the periodic boundary condition is attributed to the faces D and E. All the interior surfaces including face F that are not part of the rigid geometry and are only designated to refine the grid mesh around the blades are set as interior boundary conditions.

$$\lambda = \frac{R\Omega}{V} \tag{12}$$

where Ω is the angular speed of the rotor, R the blade radius, and V the incident free-stream airflow speed.

4. RESULTS AND DISCUSSION

To assess the performance of the proposed blade by this research, as the first step, the blade geometry used in the study of Loth et al. [1], named D2PAL, was modeled in a CAD software named CATIA, which would be considered as the reference model for further comparisons. Then, by considering identical conditions of Loth et al. [1], CFD simulation of flow around this CAD modeled blade was carried out. Finally, to attempt to implement data validation, several parameters including the turbine's power coefficient (Cp), thrust force, and the applied torque on blades were extracted and compared with the actual D2PAL [1].

4.1. Validation of the reference model

4.1.1. Evaluation of the developed torque

Figure 9 shows the generated torque at different wind speeds for the original D2PAL and its CAD modeled blade. As shown in the graph, the highest error occurs at a wind speed of 20 m/s and is reported to be 7-8 %, while the lowest deviation is reported in the rated condition of 14.125 m/s, with only 1.39 % error. Also, the mean error percentage is found to be almost 4.

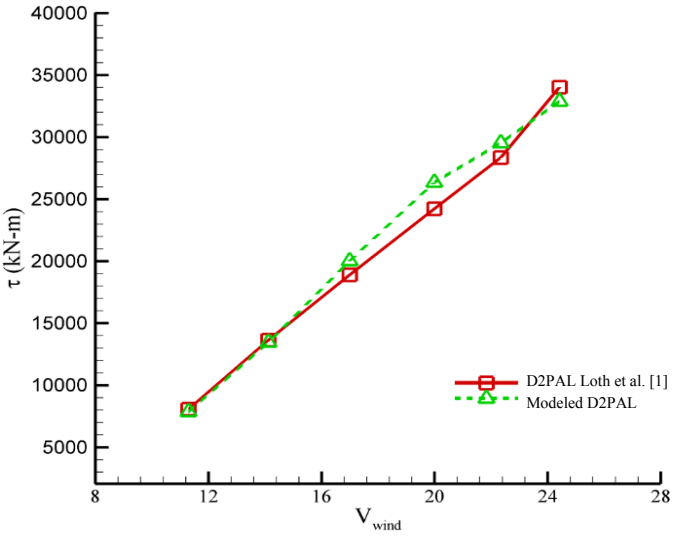

Figure 9. Developed torque as a function of wind speed

4.1.2. Evaluation of power coefficient

Evaluation of power coefficient (Cp) for the actual D2PAL and the CAD modeled blade is presented in Figure 10. With respect to the graph, generally, it can be pointed out that the

results from the modeled blade are in good agreement with the simulation results of the study established by Loth et al. [1].

In addition, Table 2 provides data regarding the deviance percentage of the calculated power coefficient for the actual D2PAL [1] and its CAD modeled rotor at the tip speed ratio of 11. According to Table 2, the lowest and highest deviations are observed at $\lambda = 14$ and 5, respectively, where computed results via FLUENT were overestimated about 0.29 % for the former and 8.78 % for the latter, compared to the experimental values. In addition, the average deviation percentage was reported to be almost 3.0 %.

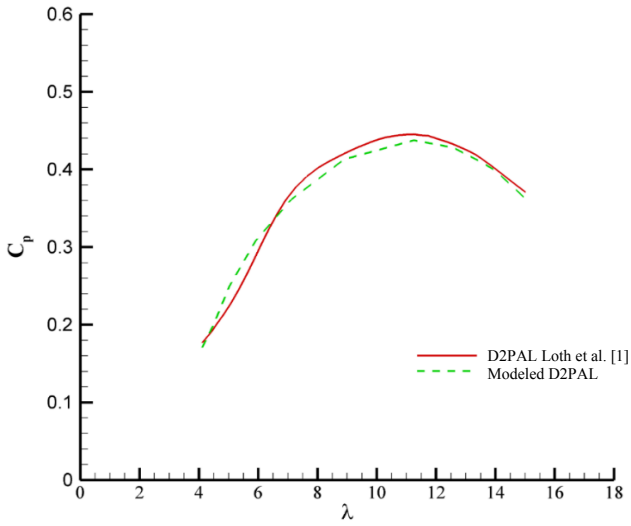

Figure 10. Power coefficient at different tip speed ratios

Table 2. Deviation percentage of calculated power coefficient at different tip speed ratios

Deviation	C_p presented by Loth et al. [1]	Calculated C_p with Fluent	(λ)
3.37 %	0.176	0.171	4.12
4.16 %	0.192	0.20	4.5
8.78 %	0.23	0.25	5
5.99 %	0.29	0.308	5.9
1.4 %	0.366	0.361	7.1
2.4 %	0.423	0.412	8.9
1.73 %	0.445	0.437	11.25
1.52 %	0.434	0.428	12.57
1.13 %	0.414	0.409	13.51
0.29 %	0.399	0.398	14
2.27 %	0.37	0.362	15

Acknowledging the precision of the above results, modeling and CFD simulations of the proposed concept, which is a bent blade with a coning angle of 17.5°, could be safely and consistently proceeded further along.

4.2. Simulation results of the proposed model

4.2.1. Assessment of performance parameters

4.2.1.1. Thrust force

A comparison between the total thrust force as a function of wind speed for the D2PAL and the bent blade is shown in Figure 11. This figure indicates that the thrust force in the D2PAL rotor is always lower than that in the bent blade for all wind speeds.

4.2.1.2. Thrust coefficient

The diagram in Figure 12 illustrates the thrust coefficient (C_T) as a function of the wind velocity for both the D2PAL and the bent blade. With a glimpse into the graph, it is worth mentioning that although the thrust coefficient has a direct linear relationship with the thrust force, changes in flow velocity have a stronger effect. This is because the thrust force has an inverse relationship with the square of the free stream velocity. Therefore, the thrust coefficient declines as the free stream speed increases.

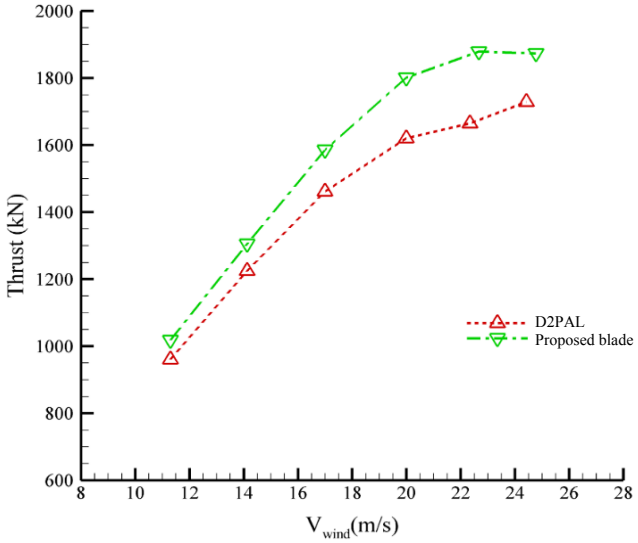

Figure 11. Total thrust force as a function of wind speed for the modeled D2PAL and the proposed blade

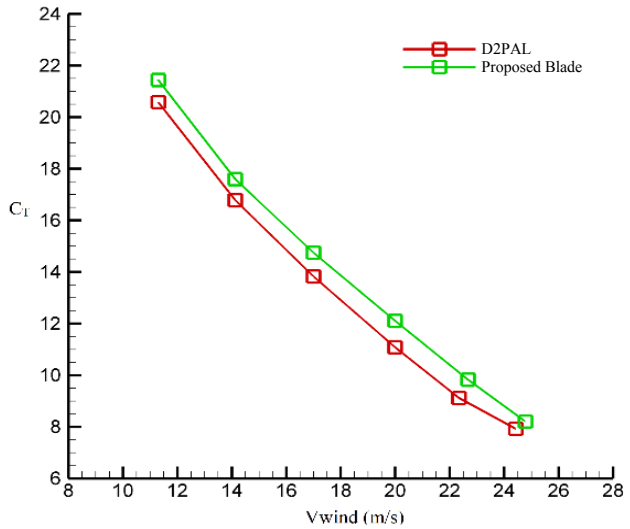

Figure 12. Thrust coefficient as a function of wind speed for the modeled D2PAL and the proposed blade

4.2.1.3. Rotor's torque

The torque developed by the proposed rotor concept as a function of wind speed is shown in Figure 13. As in the figure, as the wind speed increases, the torque exerted on the rotor also increases; however, the striking point here is that the greatest generated torque belongs to the bent blade, which in

turn can result in a higher power coefficient. The position and the magnitude of the coned angle in the bent blade geometry, which provided a longer moment arm than that of the D2PAL blade, is one of the main contributors to this increase.

4.2.1.4. Power coefficient

Figure 14 displays the results of the captured power coefficients for both of the proposed blade and the modeled D2PAL along with the D2PAL data set given by Loth et al. [1]. According to the graph in Figure 14, the proposed blade presented in this study has considerably enhanced the power coefficient compared to the D2PAL blade. The simulation results have exhibited increase rates of 13.21 % and 12.79 % in the mean power coefficient of the bent blade compared to the actual D2PAL and its modeled blade, respectively. The growth of the bent blade's swept area due to its unique bending point is responsible for this increase. Another contributing factor could be the enhancement of the airfoils' alignment with the wind flow, compared to the D2PAL blade.

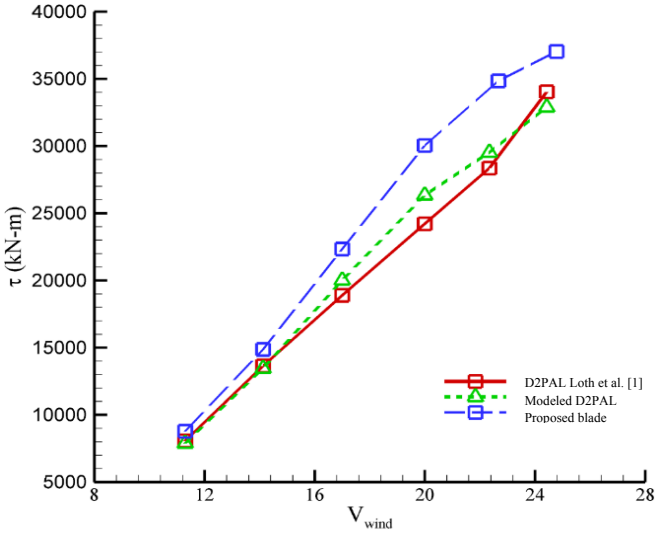

Figure 13. Developed torque as a function of wind speed for both D2PALs and the proposed blade

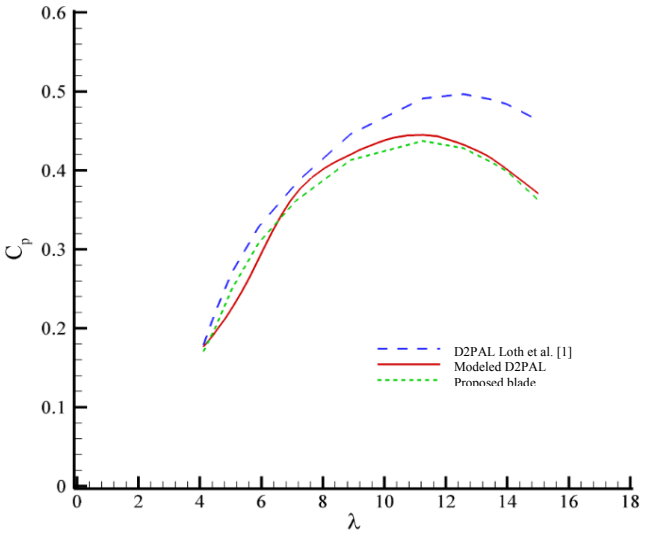

Figure 14. Power coefficient for both D2PALs and the proposed blade concept

4.2.2. Simulation of the flow field around blades

4.2.2.1. Flow velocity pattern

The flow velocity behind the two-bladed configurations is shown in Figure 15. The simulation results revealed that the decline in the flow velocity behind the proposed bent blade is, to some extent, greater than that of the coned blade. This means that the bent wind turbine is more capable of harnessing the kinetic energy of the wind based on Betz's law, which in turn results in a higher power coefficient.

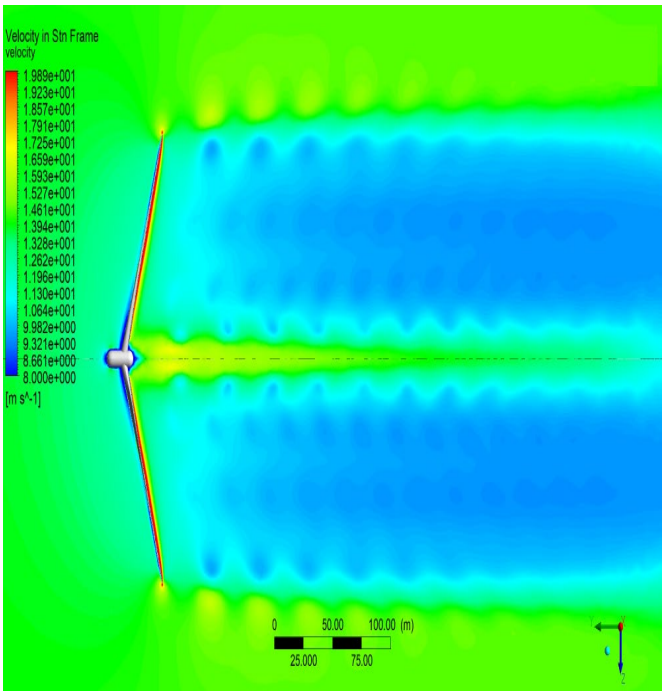

(a)

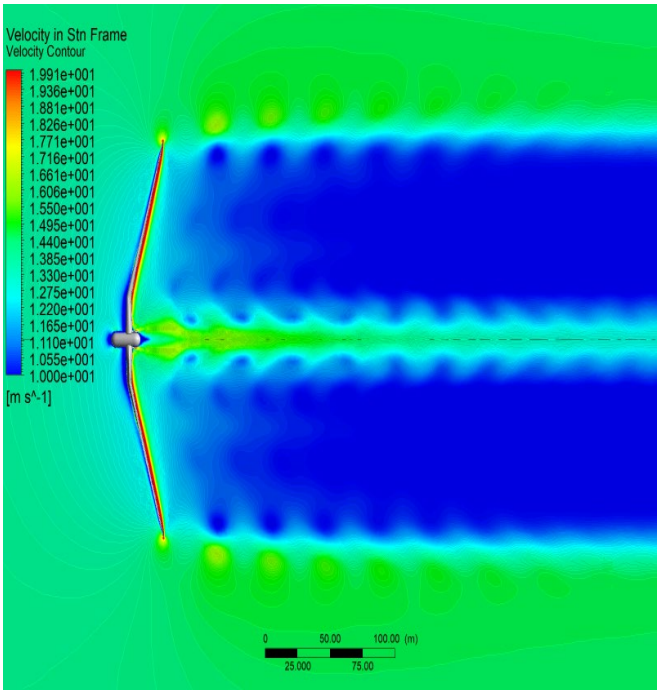

(b)

Figure 15. Comparison of flow velocity around the rotor in the rated condition (14/125 m/s) for a) the modeled D2PAL blade and b) the proposed blade

Figure 16 represents the tangential velocity vectors for both the coned and bent blades. The greatest velocity magnitude occurs at the blade's tip, while the lowest occurs at its root.

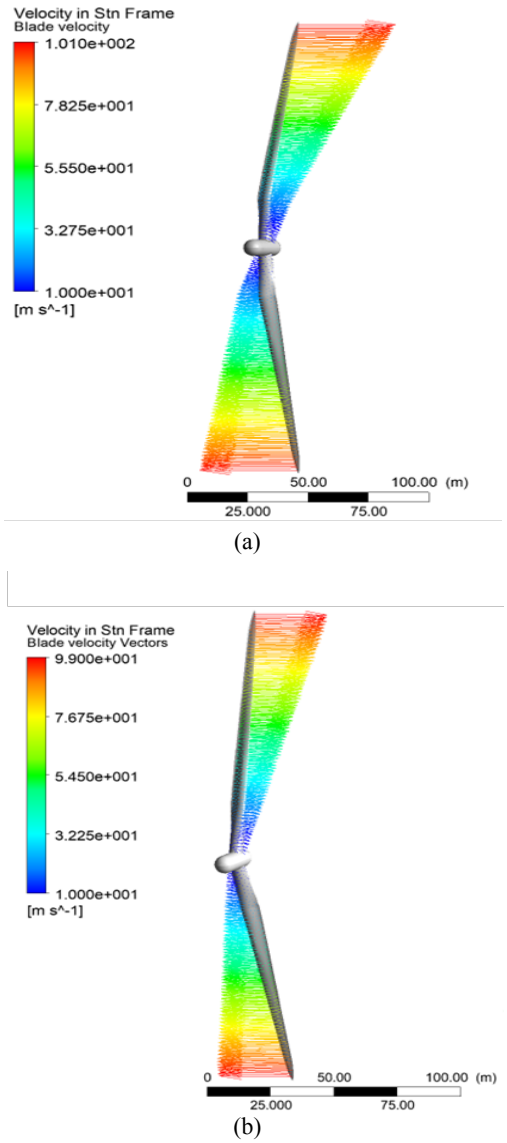

Figure 16. Comparison of tangential velocity vectors for a) the proposed blade and b) the modeled D2PAL blade

4.2.2.2. Streamlines and wake simulation

This section discusses the wake simulation results and the flow streamlines of the two different rotor configurations in rated conditions (14.125 m/s) and the rotational speed of 8.93 rpm for the rotor. In the case of wind turbines, flow streamlines twist after they collide with blades and hub. An illustration of this phenomenon for both coned and bent rotors is given in Figure 17. According to this figure, the swirling streamlines not only are formed earlier around the bent blade but also are more intense, closely tight, and tangled together. The main reason for this distinction might be the difference in the bending point of the two blades' configurations.

A comparison of the generated downstream vortices and the wakes behind the two coned and bent rotors is made, as given in Figure 18. Wake simulation results have shown that the wakes behind the bent rotor are formed closer to the rotation plane for identical free-stream velocity and rotational speed. This phenomenon is ascribed to different geometries of the two blades. As shown in Figure 18, the initial wakes form right at the tip of the blade. On the other hand, the blade tip in the proposed rotor is positioned closer to the rotation plane because the bending point in the bent blade is designed at the end of its cylindrical cross-section, while the conventional pre-aligned configuration starts right from the hub. This structure delays the formation of wakes and vortices behind the turbine.

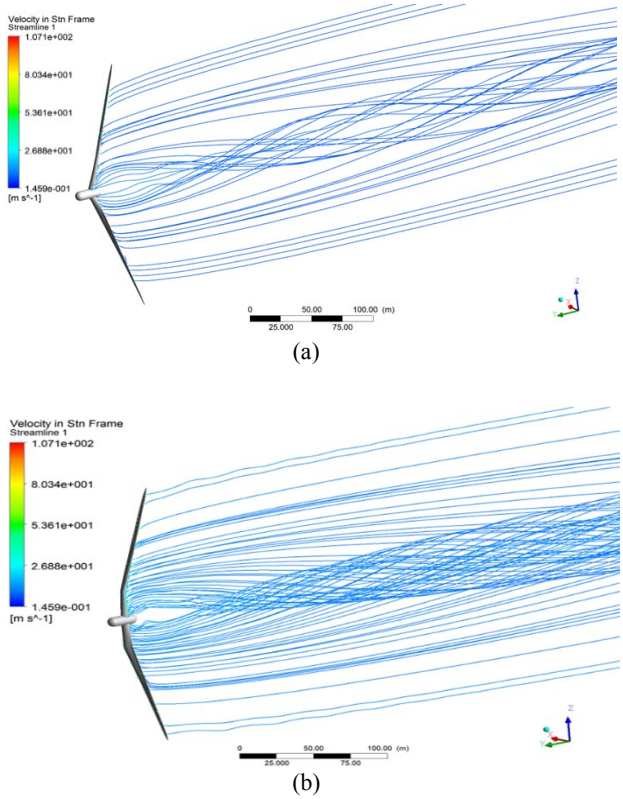

Figure 17. Comparison of streamlines behind the rotor in a) the D2PAL and b) proposed blade concept

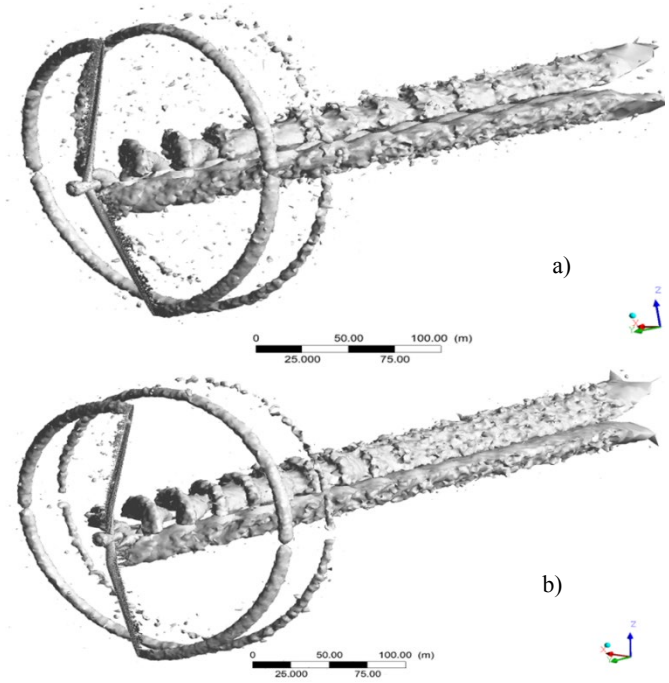

Figure 18. Isometric view of the generated wake behind the rotor at rated condition for a) Rotor with the modeled D2PAL blade, b) Rotor with the proposed blade

5. CONCLUSIONS

In this study, modeling and CFD simulation of two downwind pre-aligned turbines with different blade concepts were conducted. The first concept used as a reference model for data validation was a coned blade with a fixed downwind conceptual angled from the blade root, while the second design was a blade bent lengthwise concept proposed in this study. The latter had a coning angle of 17.5° at a particular point in the transition area between the cylindrical section and the blade's first airfoil. Both of the rotors were compared in terms of several performance parameters including power coefficient, thrust force, and applied torque on the blades.

Increased swept area led to a considerable improvement in the mean power coefficient. It was also found that the thrust force of the proposed bent blade was greater than that of the coned blade under all wind speeds. The simulation results revealed that the mean produced power by the bent rotor increased by 13.21 % compared to the reference coned rotor designs. Analyzing the induction area in front of the rotor plane displayed a greater drop in the flow velocity streaming to the bent rotor, which in turn could lead to a more efficient energy conversion for harnessing the wind power based on Betz's law. The wake simulation captured a delay in the formation of vortices behind the turbine with a coned blade, which is due to its geometrical structure.

The lengthwise bent blade rotor enjoys a higher capability to harvest wind energy at low upstream wind speeds, as the root portion of straight wind turbine blades has the main role in wind turbine power production at lower wind speeds because of the twist arrangement design.

6. ACKNOWLEDGEMENT

I would like to express my special thanks of gratitude to Shahrood University of Technology, Department of Mechanical Engineering, which supported us with high speed computers in our research process.

NOMENCLATURE

a	Axial induction factor
a'	Tangential induction factor
A , A_d	Rotor disk area
B	Number of blades
c	Chord
C , F_C	Centrifugal force
C_d	Drag coefficient
C_P	Power coefficient
C_T	Thrust coefficient
D	Drag force
F_1	Blending function
F_Q	Torque-wise force
F_R	Resultant force
G , F_G	Gravitational force
k	Turbulent kinetic energy
L	Lift force
M	Mach number
p	Pressure
P	Power
Q	Torque
R	Blade radius
t	Time
T , F_T	Thrust force
u	Flow velocity
V , U_∞	Wind speed
W	Relative wind velocity
Greek letters	
ν	Kinematic viscosity
ν_t	Kinematic eddy viscosity
μ_t	Eddy viscosity
β	Load-path angle
φ	Blade azimuthal angle
λ	Tip-speed ratio
ρ	Density
τ	Torque moment
ω	Turbulent frequency
τ_{ij}	Turbulent Reynolds stress tensor
$\dot{\beta}$	Turbulence modeling constant
β^*	Turbulence modeling constant
σ	Turbulence modeling constant
γ	Turbulence modeling constant
Ω	Angular speed of rotor
Subscripts	
3D	Three dimensional
BC	Boundary condition
BEM	Blade element momentum theory
CAD	Computer-aided design
CFD	Computational Fluid Dynamics
D2PAL	Downwind 2-Bladed Pre-Aligned Lengthened
DPAR	Downwind Pre-Aligned Rotor
LCOE	Levelized Cost of Energy
MDAR	Morphing Downwind-Aligned Rotor
SST	Shear Stress Transport
SUMR	Segmented Ultralight Morphing Rotors
SUPAR	Segmented Ultralight Pre-Aligned Rotors
WTCFD	Wind Turbine Computational Fluid Dynamics

REFERENCES

1. Loth, E., Steele, A., Qin, C., Ichter, B., Selig, M.S. and Moriarty, P., "Downwind pre-aligned rotors for extreme-scale wind turbines", ***Wind Energy***, Vol. 20, No. 7, (2017), 1241-1259. (https://doi.org/10.1002/we.2092).
2. Wingerden, J.V., Hulskamp, A., Barlas, T.K., Marrant, B., Kuik, G.V., Molenaar, D.P. and Verhaegen, M., "On the proof of concept of a smart wind turbine rotor blade for load alleviation", ***Wind Energy***, Vol. 11, (2008), 265-280. (https://doi.org/10.1002/we.264).
3. Chetan, M., Sakib, M.S., Griffith, D.T. and Yao, S., "Aero-structural design study of extreme-scale segmented ultralight morphing rotor blades", ***Proceedings of AIAA AVIATION 2019 Forum***, Dallas, Texas, (2019). (https://doi.org/10.2514/6.2019-3347).
4. Fischer, G.R., Kipouros, T. and Savill, A.M., "Multi-objective optimisation of horizontal axis wind turbine structure and energy production using aerofoil and blade properties as design variables", ***Renewable Energy***, Vol. 62, (2014), 506-515. (https://doi.org/10.1016/j.renene.2013.08.009).
5. Sartori, L., Bellini, F., Croce, A. and Bottasso, C., "Preliminary design and optimization of a 20 MW reference wind turbine", ***Journal of Physics: Conference Series***, Vol. 1037, (2018). (https://doi.org/10.1088/1742-6596/1037/4/042003).
6. Griffith, D.T. and Richards, P.W., "The SNL100-03 blade: Design studies with flatback airfoils for the Sandia 100-meter blade", Sandia National Labs, Technical report SAND2014-18129, (2014). (http://energy.sandia.gov/wp-content/gallery/uploads/dlm_uploads/1418129.pdf).
7. Deshmukh, A.P. and Allison, J.T., "Multidisciplinary dynamic optimization of horizontal axis wind turbine design", ***Structural and Multidisciplinary Optimization***, Vol. 53, (2016), 15-27. (https://doi.org/10.1007/s00158-015-1308-y).
8. Fingersh, L.J., Hand, M.M. and Laxson, A.S., "Wind turbine design cost and scaling model", National Renewable Energy Lab (NREL), Golden, Colorado, USA, (2006). (https://doi.org/10.2172/897434).
9. Loth, E., Steele, A., Ichter, B., Selig, M. and Moriarty, P., "Segmented ultralight pre-aligned rotor for extreme-scale wind turbines", ***Proceedings of AIAA Aerospace Sciences Meeting***, Nashville, Tennessee, USA, (2012). (https://doi.org/10.2514/6.2012-1290).
10. Thomsen, O.T., "Sandwich materials for wind turbine blades - Present and future", ***Journal of Sandwich Structures & Materials***, Vol. 11, (2009), 7-24. (http://dx.doi.org/10.1177/1099636208099710).
11. Thirumalai, R. and Prabhakaran, D., "Future materials for wind turbine blades - A critical review", ***Proceedings of International Conference on Wind Energy: Materials, Engineering and Policies***, Hyderabad, India, (2012).

(https://www.inderscienceonline.com/doi/abs/10.1504/IJMATEI.2014.060339).

12. Konga, C., Banga, J. and Sugiyamab, Y., "Structural investigation of composite wind turbine blade considering various load cases and fatigue life", ***Energy***, Vol. 30, (2005), 2101-2114. (http://dx.doi.org/10.1016/j.energy.2004.08.016).
13. Liao, C.C., Zhao, X.L. and Xu, J.Z., "Blade layers optimization of wind turbines using FAST and improved PISO algorithm", ***Renewable Energy***, Vol. 42, (2012), 227-233. (http://dx.doi.org/10.1016/j.renene.2011.08.011).
14. Rasmussen, F., Petersen, J.T., Vølund, P., Leconte, P., Szechenyi, E. and Westergaard, C., "Soft rotor design for flexible turbines- Final report", (1998), 1-19. (https://cordis.europa.eu/docs/projects/files/JOR/JOR3950062/47698171-6_en.pdf).
15. Tong, W., Wind power generation and wind turbine design, WIT Press, (2010). (https://www.witpress.com/books/978-1-84564-205-1).
16. Loth, E., Selig, M. and Moriarty, P., "Morphing segmented wind turbine concept", ***Proceedings of 28th AIAA Applied Aerodynamics Conference***, Chicago, Illinois, USA, (2010). (https://doi.org/10.2514/6.2010-4400).
17. Daynes, S. and Weaver, P.M., "Design and testing of a deformable wind turbine blade control surface", ***Smart Materials and Structures***, Vol. 21, No. 10, (2012). (https://doi.org/10.1088/0964-1726/21/10/105019).
18. Neal, D.A., Good, M.G. and Johnston, C.O., "Design and wind-tunnel analysis of a fully adaptive aircraft configuration", ***Proceedings of 45th AIAA/ASME/ASCE/AHS/ASC Structures, Structural Dynamics & Materials Conference***, Palm Springs, California, USA, (2004). (https://doi.org/10.2514/6.2004-1727).
19. Buhl, T., Bak, D.C., Gaunaa, M. and Andersen, P.B., "Load alleviation through adaptive trailing edge control surfaces: Adapwing overview", ***Proceedings of European Wind Energy Conference and Exhibition***, Milan, Italy, (2007). (https://www.semanticscholar.org/paper/Load-alleviation-through-adaptive-trailing-edge-Buhl-Bak/a8af7c1327cbac0796888a3aeca3d48de7dc2cf6).
20. Lachenal, X., Daynes, S. and Weaver, P.M., "Review of morphing concepts and materials for wind turbine blade applications", ***Wind Energy***, Vol. 16, (2013), 283-307. (https://doi.org/10.1002/we.531).
21. Wang, W., Caro, S.E. and Bennis, F., "Optimal design of a simplified morphing blade for fixed-speed horizontal axis wind turbines", ***Proceedings of the ASME 2012 International Design Engineering Technical Conferences & Computers and Information in Engineering Conference***, Chicago, Illinois, USA, (2012), 233-242. (https://doi.org/10.1115/DETC2012-70225).
22. Lackner, M.A. and Kuik, G.V., "A comparison of smart rotor control approaches using trailing edge flaps and individual pitch control", ***Wind Energy***, Vol. 13, (2010), 117-134. (https://doi.org/10.1002/we.353).
23. Griffith, D.T., "Structural design of the SUMR-13 wind turbine blade-Technical report M2.5.9", Advanced Research Projects Agency - Energy, (2017). (https://arpa-e.energy.gov/technologies/projects/ultra-large-wind-turbine).
24. Steele, A., Ichter, B., Qin, C., Loth, E., Selig, M. and Moriarty, P., "Aerodynamics of an ultralight load-aligned rotor for extreme-scale wind turbines", ***Proceedings of 51st AIAA Aerospace Sciences Meeting Including the New Horizons Forum and Aerospace Exposition***, Grapevine, Texas, USA, (2013). (https://doi.org/10.2514/6.2013-914).
25. Yao, S., Chetan, M. and Griffith, D.T., "Structural design and optimization of a series of 13.2 MW downwind rotors", ***Wind Engineering***, Vol. 45, No. 6, (2021), 1459-1478. (https://doi.org/10.1177/0309524X20984164).
26. Ananda, G.K., Bansal, S. and Selig, M.S., "Aerodynamic design of the 13.2 MW SUMR-13i wind turbine rotor", ***Proceedings of Wind Energy Symposium, American Institute of Aeronautics and Astronautics***, Kissimmee, Florida, USA, (2018). (https://m-selig.ae.illinois.edu/pubs/AnandaBansalSelig-2018-AIAA-Paper-2018-0994-SUMR-13i.pdf).
27. Noyes, C., Qin, C. and Loth, E., "Pre-aligned downwind rotor for a 13.2 MW wind turbine", ***Renewable Energy***, (2018), 749-754. (https://doi.org/10.1016/j.renene.2017.10.019).
28. Zalkind, D.S., Ananda, G.K. and Chetan, M., "System-level design studies for large rotors", ***Wind Energy Science***, Vol. 4, (2019), 595-618. (https://doi.org/10.5194/wes-4-595-2019).
29. Noyes, C., Qin, C. and Loth, E., "Ultralight morphing rotor for extreme-scale wind turbines", ***Proceedings of AIAA SciTech Forum***, (2017), 1-6. (https://doi.org/10.2514/6.2017-0924).
30. Ichter, B., Steele, A., Loth, E., Moriarty, P. and Selig, M., "A morphing downwind-aligned rotor concept based on a 13 MW wind turbine", ***Wind Energy***, Vol. 19, (2016), 625-637. (https://doi.org/10.1002/we.1855).
31. Noyes, C., Qin, C. and Loth, E., "Analytic analysis of load alignment for coning extreme-scale rotors", ***Wind Energy***, Vol. 23, (2020), 357-369. (https://doi.org/10.1002/we.2435).
32. Qin, C., Loth, E., Zalkind, D.S., Pao, L.Y., Yao, S., Griffith, D.T., Selig, M.S. and Damiani, M.S., "Downwind coning concept rotor for a 25 MW offshore wind turbine", ***Renewable Energy***, Vol. 156, (2020), 314-327. (https://doi.org/10.1016/j.renene.2020.04.039).
33. Yao, S., Chetan, M., Griffith, D.T., Mendoza, A.S., Selig, M.S. and Martin, D., "Aero-structural design and optimization of 50 MW wind turbine with over 250 m blades", ***Wind Engineering***, (2021). (https://doi.org/10.1177/0309524X211027355).
34. Bortolotti, P., Kapila, A. and Bottasso, C.L., "Comparison between upwind and downwind designs of a 10 MW wind turbine rotor", ***Wind Energy Science***, Vol. 4, (2019), 115-125. (https://doi.org/10.5194/wes-4-115-2019).
35. Ichter, B., Steele, A., Loth, E. and Moriarty, P., "Structural design and analysis of a segmented ultralight morphing rotor (SUMR) for extreme-scale wind turbines", ***Proceedings of 42nd AIAA Fluid Dynamics Conference***, New Orleans, Louisiana, USA, (2012). (https://doi.org/10.2514/6.2012-3270).
36. Crawford, C., "Parametric variations of a coning rotor wind turbine", ***Proceedings of 46th AIAA Aerospace Sciences Meeting and Exhibit***, Reno, Nevada, USA, (2008). (https://doi.org/10.2514/6.2008-1340).
37. Ning, A. and Petch, D., "Integrated design of downwind land-based wind turbines using analytic gradients", ***Wind Energy***, Vol. 19, (2016), 2137-2152. (https://doi.org/10.1002/we.1972).
38. Tossas, L.M. and Leonardi, S., "Wind turbine modeling for computational fluid dynamics", National Renewable Energy Laboratory, Technical report No. NREL/SR- 5000-55054, (2013). (https://www.nrel.gov/docs/fy13osti/55054.pdf).
39. Réthoré, P., "Thrust and wake of a wind turbine: Relationship and measurements", Master's Thesis, Technical University of Denmark, (2006). (https://www.mek.dtu.dk/-/media/Institutter/Mekanik/Sektioner/FVM/uddannelse/eksamensprojekt/mastertheses-fm/pierrerethore2006.ashx?hash=4E37E5F71D60845E67D3A018D7373297BA54C4E3&la=da).
40. Burton, T., Sharpe, D., Jenkins, N. and Bossanyi, E., Wind energy handbook, John Wiley & Sons, (2001). (https://books.google.com/books/about/Wind_Energy_Handbook.html?id=4UYm893y-34C).
41. Chu, Y.J., Lam, H.F. and Peng, H.Y., "Numerical investigation of the power and self-start performance of a folding-blade horizontal axis wind turbine with a downwind configuration", ***International Journal of Green Energy***, Vol. 19, No. 1, (2021), 28-51. (https://doi.org/10.1080/15435075.2021.1930003).
42. Betz, A., "The maximum of the theoretically possible exploitation of wind by means of a wind motor", ***Wind Engineering***, Vol. 37, (2013), 441-446. (https://www.jstor.org/stable/43857254).
43. Menter, F.R., "Two-equation eddy-viscosity turbulence models for engineering applications", ***AIAA Journal***, Vol. 32, (1994), 1598-1605. (https://doi.org/10.2514/3.12149).
44. Wilcox, D.C., Turbulence modeling for CFD, Second edition, DCW Industries, (1994). (https://books.google.com/books?id=VwlRAAAAMAAJ&q).
45. Launder, B.E. and Spalding, D.B., Lectures in mathematical models of turbulence, Academic Press, (1972). (https://books.google.com/books?id=61iqAAAAIAAJ&dq).
46. Griffith, D.T. and Ashwill, T.D., "The Sandia 100-meter all-glass baseline wind turbine blade:SNL100-00", Sandia National Laboratories, Albuquerque, report No. SAND2011-3779, (2011). (https://energy.sandia.gov/wp-content/gallery/uploads/SAND2011-3779.pdf).
47. ANSYS. 12.0 user's guide, Ansys Incorporayion, (2009). (https://www.afs.enea.it/project/neptunius/docs/fluent/html/ug/main_pre.htm), (Accessed: 16 July 2009).